



Occurrence of mixed-mode oscillations in a system consisting of a Van der Pol system and a Duffing oscillator with two potential wells

Weipeng Lyu · Shaolong Li · Juanjuan Huang · Qinsheng Bi

Received: 26 May 2023 / Accepted: 15 January 2024 / Published online: 27 February 2024
© The Author(s), under exclusive licence to Springer Nature B.V. 2024

Abstract Mixed-mode oscillations (abbreviated as MMOs) belong to a typical kind of fast/slow dynamical behavior, and how to investigate the mechanism is an important problem in nonlinear dynamics. In this paper, we explore the MMOs induced by the bifurcation delay phenomenon and twist of the trajectories in space based on a coupled system consisting of a Van der Pol system and a Duffing oscillator with two potential wells. Regarding the low-frequency external excitation as a generalized state variable, we obtain the traditional fast and slow subsystems. Applying the equilibrium analysis and bifurcation theory, the stability critical conditions of the equilibrium and the generation conditions of fold and Hopf bifurcation are also presented. To analyze the critical conditions clearly, the two-parameter bifurcation and one-parameter bifurcation diagrams are performed by using numerical simulation method. The bifurcation characteristics are studied, especially the effects of parameter δ on the bifurcation structures. We find that the fast subsystem performs different dynamical behaviors such as fold bifurcation of limit cycles, period-doubling bifurcations, inverse-period-doubling

bifurcations and chaos, when parameter δ is taken at different values. By using phase diagrams, time series, maximum Lyapunov exponent diagrams, three-dimensional phase diagrams and superimposed diagrams, the mechanisms of the MMOs are investigated numerically in detail. The Hopf bifurcation delay can lead the trajectories to arrive at the vector fields of the equilibrium point and limit cycles. In addition, the chaotic behaviors can be found on the route of period doubling, which lead to the chaotic spiking-state-oscillations types. Our findings are helpful to understand the generation of the MMOs and intensify the understanding of some special dynamical behaviors on the MMOs.

Keywords MMOs · Coupled Van der Pol–Duffing system · Bifurcation · Hopf bifurcation delay · Chaos

1 Introduction

In the fields of science and engineering, many nonlinear systems often involve multiple timescale effect, such as nervous systems [1, 2], circuit models [3, 4], energy harvesters [5, 6] and laser oscillators [7, 8]. MMOs, as a typical dynamical behavior induced by the multiple timescale effect, represented by an alternation between the small-amplitude static oscillations (SASOs) and large-amplitude dynamical

W. Lyu (✉) · S. Li · J. Huang
School of Mathematics and Statistics, Yancheng Teachers
University, Yancheng 224002, China
e-mail: Lvwp@yctu.edu.cn

Q. Bi
Faculty of Civil Engineering and Mechanics, Jiangsu
University, Zhenjiang 212013, China

waves (LADWs), are often observed in many fast/slow nonlinear systems [9–11]. Generally, the SASOs correspond to the trajectory moving in the vector fields of the stable equilibrium points or the small-amplitude limit cycles, while the LADWs are corresponding to the trajectory vibrating in the attraction domain of the large-amplitude limit cycles. Two important dynamical behaviors related to the MMOs, i.e., the dynamical behaviors of the SASOs that result in the LADWs and the dynamical behavior of the LADWs that result in the SASOs, can be noted [12–14]. Moreover, the SASOs are commonly known as the quiescent state, and the LADWs are referred to the spiking state.

The MMOs were first discovered by Van der Pol in 1926 [15], but due to the lack of the effective analytical method, the study of the MMOs was not received sufficient attention at that time. In 1952, Hodgkin and Huxley established a nonlinear ordinary differential system with three fast and one slow subsystems, which could successfully reconstruct the MMOs in the experimental observations. From then on, the research on the MMOs has been becoming a hot topic. Many analytical methods have been introduced to explore the mechanisms of different MMOs, such as experimental analysis [16, 17], numerical simulation [18, 19], geometrical singular perturbation method [20, 21] and fast/slow analysis method [22, 23]. Based on these methods, many different patterns of the MMOs are investigated. For example, Sharma et al. [24] reported the aperiodic MMOs and synchronized MMOs in the experiments on an active camphor rotor. Liu and Liu [25] investigated the MMOs induce by the canard phenomenon by using the geometrical singular perturbation method. Kouayep et al. [26] explored the mechanisms of the periodic MMOs, chaotic MMOs and chaotic pulse-package vibrations experimentally. Bao et al. [27] discussed the generation of the chaotic MMOs, periodic MMOs and chaotic tonic-spiking in the 3D Morris-Lecar neuron model. Most of the MMOs that have been obtained are induced by the time-domain multiscale effect, i.e., the system contains some state variables that vary at quite different change rates. However, for the systems with frequency multiscale effect, the MMOs also can be created when the excitation frequency is much smaller than the system natural frequency [28, 29]. Since there are no obvious fast and slow subsystems in the coupled systems, the standard fast/slow analysis method cannot be directly used to

explore the mechanism of such MMOs. In recent years, an improved fast/slow analysis method is proposed to investigate the MMOs induced by the frequency multiscale effect [30]. The basic idea of the improved fast/slow analysis method is that the low-frequency excitation can be regarded as a slow state variable since it changes very slowly in each period of the MMOs, and the whole system is treated as a fast subsystem, thus establishing a time-domain multiscale system formally. Based on this method, the MMOs induced by the frequency multiscale effect have been explored deeply. For example, Huang and Bi [31] studied the MMOs in a high-dimensional system, and the 2-D MMOs with single-mode, two-mode and three-mode were presented. Kpomahou et al. [32] explored the existence of the MMOs and horseshoe chaos in a mixed Rayleigh-Lienard system, where the MMOs were asymmetric “fold/Hopf” type, asymmetric “fold/fold” type and asymmetric “Hopf/Hopf” type. Vijay et al. [33] reported the supercritical pitchfork/fold MMOs and supercritical pitchfork MMOs in the Lienard system with low-frequency excitation. Oyeleke et al. [34] investigated the MMOs induced by the pulse-shaped explosions, and they found that the MMOs can exhibit the cascading characteristics. Even though some achievements have been made, some problems still need to be investigated, such as possible routes to the periodic or chaotic MMOs, possible factors causing the transitions between the spiking states and quiescent states, the effect of the low-frequency excitations on the dynamical evolutions of the different MMOs and the mechanism of the MMOs in the high-dimensional systems.

In this paper, we focus on the MMOs in a system consisting of a Van der Pol system and a Duffing oscillator with two potential well. Two routes to the MMOs, namely, the bifurcation delay phenomenon and twist of the trajectories in space, are observed. Based on that, six different MMOs, i.e., “fold/fold” MMOs, “delayed supHopf/fold-fold/fold” MMOs, “fold/inverse-period-4-inverse-period-twofold limit cycle” chaotic MMOs, “fold/inverse-period-8/supHopf” chaotic MMOs, “fold/delayed fold limit cycle” chaotic MMOs and “fold/fold limit cycle” periodic MMOs, are investigated by using the phase diagrams, time series, maximum Lyapunov exponent diagrams and fast/slow analysis method. The goal of this paper has threefold. First, we present two

interesting routes to the MMOs, and several new MMOs are proposed. Second, we show the effect of a typical parameter on the bifurcation structures, stable attractors, spiking states and MMOs. Third, we deepen the applications of the improved fast/slow analysis method in the mechanism analysis of the MMOs induced by the frequency-domain multiscale effect.

The rest of this paper is organized as follows. The mathematical equation of the system consisting of a Van der Pol oscillator and a Duffing oscillator with two potential wells is presented in Sect. 2. In the following section, bifurcation analyses of the system are provided. Next, based on the bifurcation delay phenomenon and twist of trajectories in space, six different MMOs are proposed and revealed by phase diagram, time series, superposition diagrams between the bifurcation diagrams and transformation phase diagrams, and Lyapunov exponent in Sect. 4. Finally, Sect. 5 concludes the results of the whole paper.

2 Mathematical description of the coupled system

In this paper, we consider the MMOs in a system consisting of a Van der Pol system and a Duffing oscillator with two potential wells [35]. The mathematical equation of the coupled system is presented as

$$\frac{d^2x}{dt^2} - \mu(1 - x^2)\frac{dx}{dt} + x - k(y - x) = 0, \tag{1a}$$

$$\begin{aligned} \frac{d^2y}{dt^2} + \alpha\frac{dy}{dt} - y + \delta y^2 + \varepsilon y^3 - k\left(\frac{dx}{dt} - \frac{dy}{dt}\right) \\ = f \cos(\omega t), \end{aligned} \tag{1b}$$

where μ and ε are taken at real positive values to control the system nonlinearities. α and k indicate the dissipation and the coupling coefficient. f and ω denote the amplitude and frequency of external excitation. By introducing auxiliary variables $m = \frac{dx}{dt}$ and $n = \frac{dy}{dt}$, system (1) can be rewritten into a standard four-dimensional ordinary differential nonlinear equation

$$\dot{x} = m, \tag{2a}$$

$$\dot{m} = k(y - x) - x + \mu(1 - x^2)m, \tag{2b}$$

$$\dot{y} = n, \tag{2c}$$

$$\dot{n} = f \cos(\omega t) + k(m - n) - \varepsilon y^3 - \delta y^2 + y - \alpha n. \tag{2d}$$

System (1) has many physical scenarios and is studied by many researchers. For example, Wofo et al. [36] studied the analytic solutions of system (1) in both nonresonant and resonant cases and observed chaos behaviors by Shilnikov and numerical simulation. Kadji and Yamapi [37] used Whittaker method and the Floquet theory to study the general synchronization dynamics of system (1). Kuznetsov et al. [38] discussed the synchronization problem of system (1) with inertial and dissipative coupling. Liu and Zhang [39] analyzed the Bogdanov–Takens and triple zero bifurcations for system (1) with $Z(2)$ symmetry.

To analyze the mechanisms of different MMOs, we assume that the frequency of the external excitation ω satisfies $0 < \omega < \ll 1$, and then two timescale phenomenon appears in the coupled model for the case of $\frac{\omega}{\omega_0} \leq 0.1$ (ω_0 is the natural frequency of system (1) and we fix it at 1 throughout the paper). Because ω is small, the external excitation $f \cos(\omega t)$ varies slowly in each period $\frac{2\pi}{\omega}$, it can be regarded as a slow-changing parameter θ that changes in the interval of $[-1, 1]$. Then, system (2) is transformed into

$$\dot{x} = m, \tag{3a}$$

$$\dot{m} = k(y - x) - x + \mu(1 - x^2)m, \tag{3b}$$

$$\dot{y} = n, \tag{3c}$$

$$\dot{n} = \theta + k(m - n) - \varepsilon y^3 - \delta y^2 + y - \alpha n. \tag{3d}$$

By choosing the appropriate parameter values, MMOs can be observed in system (3) due to the two timescale effect, as displayed in Fig. 1, from which we can see that there are some differences among them, such as the number of the spiking-state-oscillations in every cycle and the intuitive shapes of the MMOs. The differences suggest that the generation of these MMOs may be different. To present the mechanism of these MMOs, different bifurcation critical conditions are provided in the next section.

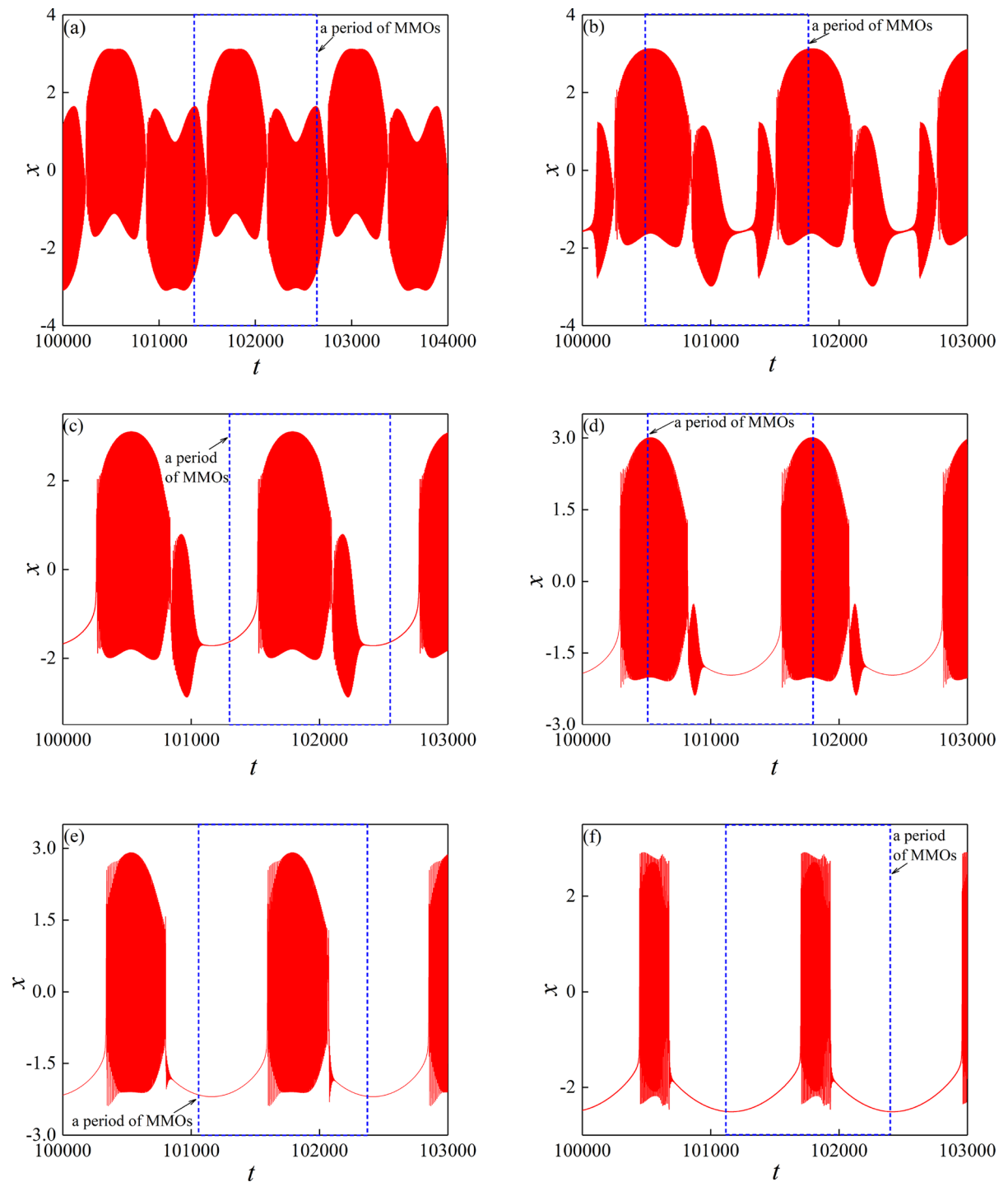


Fig. 1 Time domain responses of the MMOs for $\mu = 0.5, k = 3, \varepsilon = 1, \alpha = 0.5, f = 5$ and $\omega = 0.005$. **a** $\delta = 0.1$; **b** $\delta = 0.6$; **c** $\delta = 0.9$; **d** $\delta = 1.5$; **e** $\delta = 2$; **f** $\delta = 2.6$

3 Bifurcation analyses of the coupled system

3.1 Stability conditions

In order to obtain the equilibrium points of Eqs. 3(a), (b), (c) and (d), let the right sides of Eqs. 3(a), (b), (c) and (d) be equal to zero, we have

$$0 = m, \tag{4a}$$

$$0 = k(y - x) - x + \mu(1 - x^2)m, \tag{4b}$$

$$0 = n, \tag{4c}$$

$$0 = \theta + k(m - n) - \varepsilon y^3 - \delta y^2 + y - \alpha n. \tag{4d}$$

It can be easily found that the equilibrium points satisfy $ky = kx + x$ and $\varepsilon y^3 + \delta y^2 - y - \theta = 0$. To simplify the analysis process, all the parameters are not equal to zero in this paper. Then, the equilibrium points can be written as $E(x_0, y_0)$, where $x_0 = \frac{ky_0}{k+1}$ and y_0 is determined by $\varepsilon y_0^3 + \delta y_0^2 - y_0 - \theta = 0$.

The stabilities of $E(x_0, y_0)$ can be obtained by linearization theory and stability theory. We linearize system (3) at $E(x_0, y_0)$, the Jacobian matrix is presented as

$$\begin{aligned}
 J &= \begin{pmatrix} \frac{\partial \dot{x}}{\partial x} & \frac{\partial \dot{x}}{\partial m} & \frac{\partial \dot{x}}{\partial y} & \frac{\partial \dot{x}}{\partial n} \\ \frac{\partial \dot{m}}{\partial x} & \frac{\partial \dot{m}}{\partial m} & \frac{\partial \dot{m}}{\partial y} & \frac{\partial \dot{m}}{\partial n} \\ \frac{\partial \dot{y}}{\partial x} & \frac{\partial \dot{y}}{\partial m} & \frac{\partial \dot{y}}{\partial y} & \frac{\partial \dot{y}}{\partial n} \\ \frac{\partial \dot{n}}{\partial x} & \frac{\partial \dot{n}}{\partial m} & \frac{\partial \dot{n}}{\partial y} & \frac{\partial \dot{n}}{\partial n} \end{pmatrix} \\
 &= \begin{pmatrix} 0 & 0 & 1 & 0 \\ -(k+1) & k & \mu(1-x_0^2) & 0 \\ 0 & 0 & 0 & 1 \\ 0 & -3\varepsilon y_0^2 - 2\delta y_0 + 1 & k & -k - \alpha \end{pmatrix}. \tag{5}
 \end{aligned}$$

The related characteristic equation is displayed as $a_0\lambda^4 + a_1\lambda^3 + a_2\lambda^2 + a_3\lambda + a_4 = 0$, where $a_0 = 1, a_1 = \alpha, a_2 = -k^2 - k - k\alpha, a_3 = k^2 + (\mu - \mu x_0^2)(3\varepsilon y_0^2 + 2\delta y_0 - 1)$ and $a_4 = -(k+1)(3\varepsilon y_0^2 + 2\delta y_0 - 1)$. Based on the Routh–Hurwitz rule [40], we know that $E(x_0, y_0)$ is stable when all the following conditions are satisfied as $\Delta_0 = a_0 = 1 > 0$,

$$\Delta_1 = a_1 = \alpha > 0, \quad \Delta_2 = \det \begin{bmatrix} a_1 & a_0 \\ a_3 & a_2 \end{bmatrix} > 0 \quad \text{and}$$

$$\Delta_3 = \det \begin{bmatrix} a_1 & a_0 & 0 \\ a_3 & a_2 & a_1 \\ 0 & a_4 & a_3 \end{bmatrix} > 0. \text{ If the stable conditions}$$

are changed, different bifurcation patterns will emerge.

3.2 Generation conditions of fold bifurcation and Hopf bifurcation

When the parameters satisfy $a_4 = -(k+1)(3\varepsilon y_0^2 + 2\delta y_0 - 1) = 0$, the characteristic equation is written as $a_0\lambda^4 + a_1\lambda^3 + a_2\lambda^2 + a_3\lambda = 0$, and one of the roots is given by $\lambda_1 = 0$ that means the appearance of fold bifurcation.

On the other hand, we assume that the roots of the characteristic equation have the following form of $\lambda = \pm\omega_1 i$, bringing $\lambda = \pm\omega_1 i$ into the characteristic equation and eliminating the auxiliary parameter ω_1 , we can obtain the Hopf bifurcation conditions displayed as $a_1^3 - a_1 a_2 a_3 + a_1^2 a_4 = 0$.

A typical two-parameter bifurcation diagram related to θ and δ for chosen parameters $\mu = 0.5, k = 3, \alpha = 0.5, \varepsilon = 1, f = 5$ and $\omega = 0.005$ is displayed in Fig. 2a which is obtained by the Matcont software [41]. There are twofold bifurcation curves and two Hopf bifurcation curve, and fold-1 curve is close to Hopf2 curve. Moreover, two general-Hopf bifurcation points can be observed, which lead to the transitions in the types of Hopf bifurcations. Based on the positions of different bifurcation curves and the types of Hopf bifurcations, we can divide the whole plane into five areas, i.e., A, B, C, D and E. In each area, we can choose a typical parameter value of δ to investigate the bifurcation characteristics.

In area A, we choose $\delta = 0.1$ as a representative to explore the bifurcation structure, the related bifurcation diagram is shown in Fig. 2b. Twofold bifurcation points $LP1$ and $LP2$ divide the entire equilibrium point curve into three sections named $E1, E0$ and $E2$. For $E1$, it is stable in the interval of $(LP1, \text{sup Hopf1})$, and it becomes unstable via the supercritical Hopf bifurcation sup Hopf1 , resulting in the occurrence of a stable limit cycle $LC1$ at the same time. For $E0$, it is always unstable in the interval of $(LP1, LP2)$. For $E2$, it is stable in the interval of $(\text{sup Hopf2}, LP2)$, and it turns to be unstable via the supercritical Hopf bifurcation sup Hopf2 , resulting in the generation of the other stable limit cycle $LC2$ simultaneously. While for

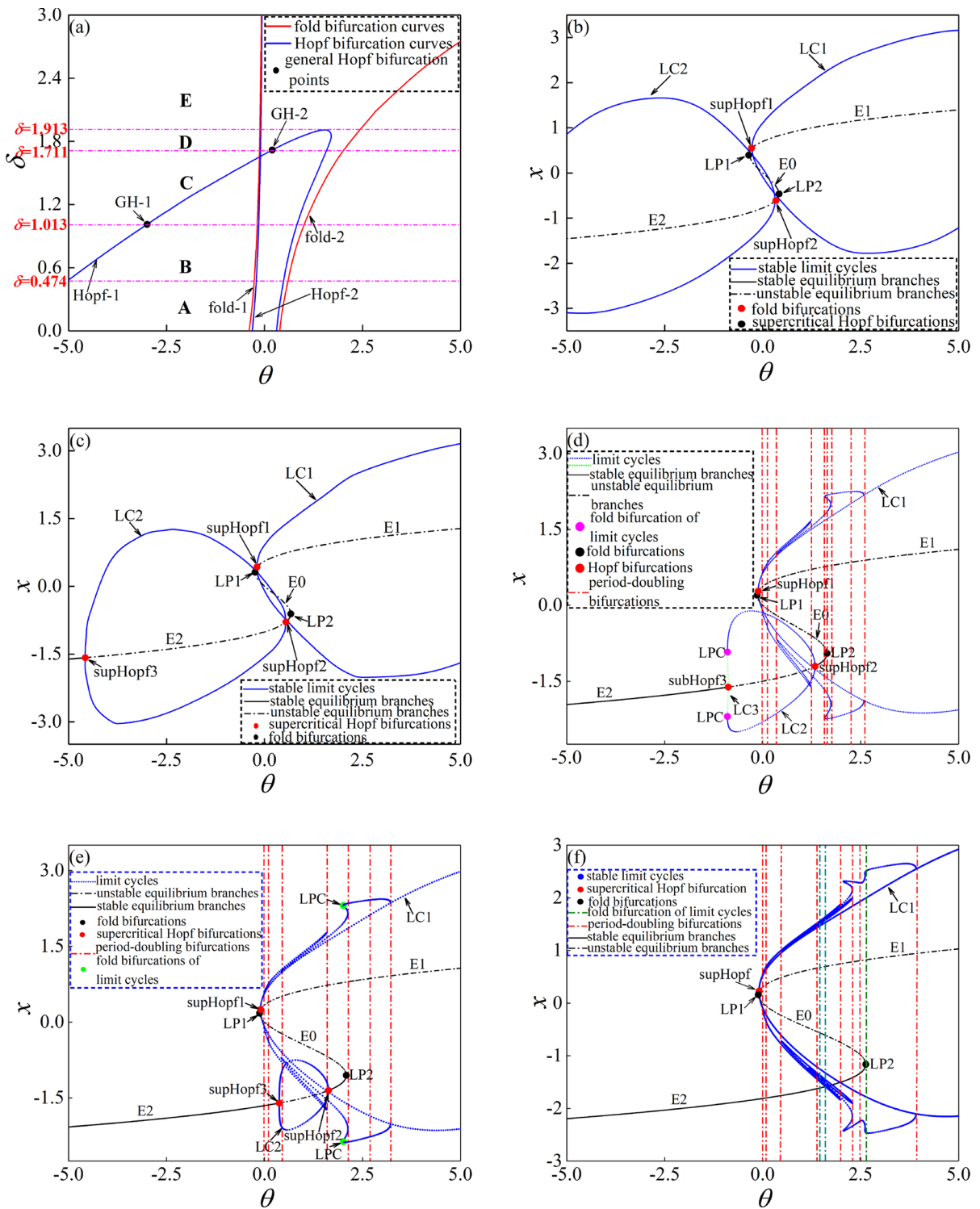


Fig. 2 Bifurcations characteristics for the chosen parameters $\mu = 0.5, k = 3, \alpha = 0.5, \varepsilon = 1, f = 5$ and $\omega = 0.005$. **a** Two-parameter bifurcation diagram corresponding to θ and δ ; **b**

Bifurcation diagram for $\delta = 0.1$; **c** Bifurcation diagram for $\delta = 0.6$; **d** Bifurcation diagram for $\delta = 1.5$; **e** Bifurcation diagram for $\delta = 1.75$; **f** Bifurcation diagram for $\delta = 2$

the stable limit cycles $LC1$ and $LC2$, they disappear at the points of sup Hopf1 and sup Hopf2 , respectively.

In area B, $\delta = 0.6$ is taken as a representative to study the bifurcation characteristics, the corresponding bifurcation diagram is displayed in Fig. 2c. The entire equilibrium curve can be divided into three sections by the fold bifurcations $LP1$ and $LP2$ obviously. On the upper branch, $E1$ is stable in the interval of $(LP1, \text{sup Hopf1})$ and becomes unstable via the supercritical Hopf bifurcation sup Hopf1 , and a stable limit cycle $LC1$ is created simultaneously. On the lower branch, $E2$ is stable in the intervals of $[-5, \text{sup Hopf3})$ and $(\text{sup Hopf2}, LP2)$, and it turns to unstable in the interval of $(\text{sup Hopf3}, \text{sup Hopf2})$. The stabilities of $E2$ are switched by two supercritical Hopf bifurcations sup Hopf2 and sup Hopf3 . While on the middle branch, $E0$ is always unstable. Moreover, the stable limit cycle $LC1$ disappears at the point of sup Hopf1 , and the stable limit cycle $LC1$ disappears at the points of sup Hopf2 and sup Hopf3 .

$\delta = 1.5$ is chosen as a typical parameter to study the dynamic characteristics in area C, the bifurcation diagram is presented in Fig. 2d. Twofold bifurcation points $LP1$ and $LP2$ separate the whole equilibrium branches into three parts, i.e., $E1$, $E0$ and $E2$. On the lower curve, $E2$ is stable in the intervals $[-5, \text{subHopf3})$ and $(\text{sup Hopf2}, LP2)$, it becomes unstable on a subcritical Hopf bifurcation subHopf3 , and resulting in the generation of an unstable limit cycle $LC3$. $E2$ also turns to unstable on a supercritical Hopf bifurcation sup Hopf2 , and leading to the production of the stable limit cycle $LC2$. Then, $LC3$ and $LC2$ collide with each other, and they disappear at the fold bifurcations of limit cycles LPC . On the upper curve, $E1$ is stable in the interval of $(LP1, \text{sup Hopf1})$ and becomes unstable on the supercritical Hopf bifurcation sup Hopf1 , and a limit cycle $LC1$ is created. In particular, a series of period-doubling bifurcations of $LC1$ can be observed. While on the middle curve, $E0$ is always unstable.

In area D, we select $\delta = 1.75$ as a typical parameter to explore the dynamical characteristics, the related bifurcation map is shown in Fig. 2e. The entire equilibrium curve is separated by the fold bifurcation points $LP1$ and $LP2$. On the lower curve, $E2$ gets its stability in the intervals of $[-5, \text{sup Hopf3})$ and $(\text{sup Hopf2}, LP2)$, and it turns to unstable in the interval of $(\text{sup Hopf3}, \text{sup Hopf2})$. The stable attractor in the interval of $(\text{sup Hopf3}, \text{sup Hopf2})$ is a

stable limit cycle $LC2$. On the upper curve, $E1$ gets its stability in the interval of $(LP1, \text{sup Hopf1})$, and it becomes unstable on a supercritical Hopf bifurcation sup Hopf1 , resulting in the generation of the limit cycle $LC1$. Moreover, a series of period-doubling bifurcation points corresponding to $LC1$ can be seen, and the stability of $LC1$ is changed by the fold bifurcations of limit cycles LPC . While on the middle curve, $E0$ is always unstable.

At last, we choose $\delta = 2$ as a typical parameter to analyze the bifurcation characteristics in area E, the relating bifurcation diagram is presented in Fig. 2f. Twofold bifurcations $LP1$ and $LP2$ separate the entire equilibrium curve into three parts, namely, the upper branch, the middle branch and the lower branch. $E2$ is always stable on the lower branch and $E0$ is always unstable on the middle branch. While on the upper curve, $E1$ obtains its stability in the interval of $(LP1, \text{sup Hopf})$ and turns to unstable in the interval of $(LP1, \text{sup Hopf})$. In addition, a limit cycle $LC1$ is produced on the supercritical Hopf bifurcation sup Hopf , and the stability of $LC1$ is transformed by a series of fold bifurcations of limit cycles.

4 Generation of different MMOs

In this section, different MMOs induced by different bifurcation structures in each area will be presented by using fast/slow analysis, phase diagram, time series and Lyapunov exponent. In addition, MMOs induced by bifurcation delay phenomenon are also studied.

4.1 “Fold/fold” MMOs

Firstly, we investigate the MMOs in area A, the parameter values are taken at $\mu = 0.5$, $k = 3$, $\alpha = 0.5$, $\varepsilon = 1$, $f = 5$, $\omega = 0.005$ and $\delta = 0.1$. From the corresponding diagrams Fig. 3a, b, we can see that the MMOs are generated by the trajectory moving around two stable limit cycle attractors. Overlapping the diagram on the plane of (θ, x) and $(z, 5 \cos(0.005t), w)$ onto the bifurcation diagram, we can obtain a clear idea on the mechanism of such MMOs. The superposition diagram is plotted in Fig. 4.

Assuming θ slowly changes from its largest value $+5$, the trajectories move violently around the stable limit cycle $LC1$, forming the spiking-state-oscillations-1. As θ arrives at the point sup Hopf1 , the

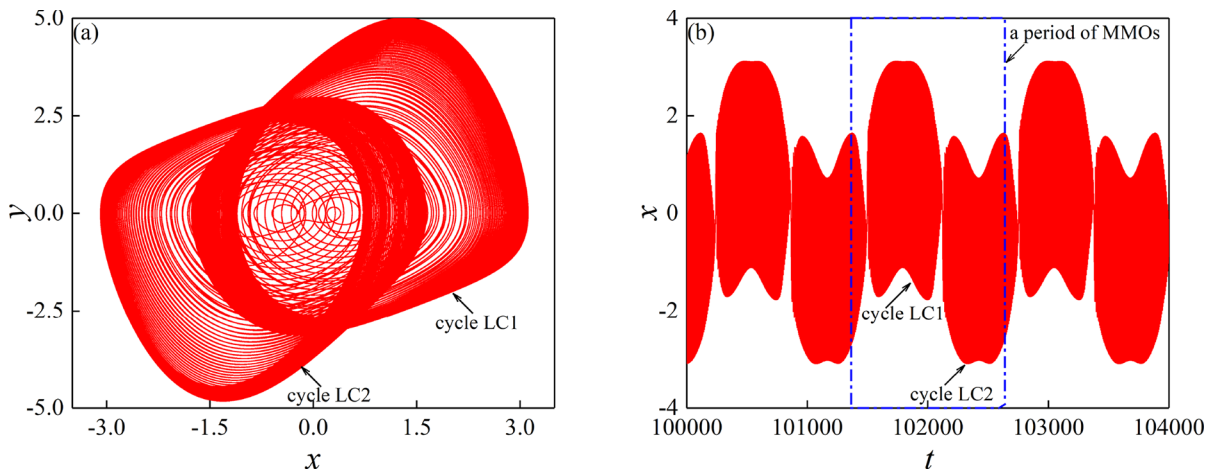


Fig. 3 The corresponding diagrams for the fixed parameters are $\mu = 0.5, k = 3, \alpha = 0.5, \varepsilon = 1, f = 5, \omega = 0.005$ and $\delta = 0.1$. **a** Diagram projected onto the (x, y) plane; **b** time histories on the plane of (t, x)

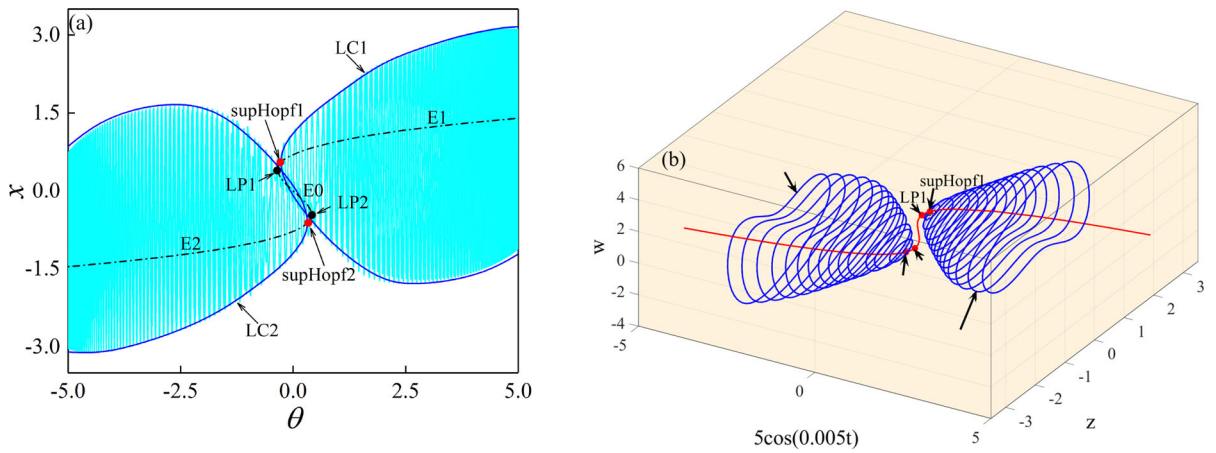


Fig. 4 The superposition diagram between the phase diagram and the bifurcation diagram. **a** Two-dimensional views of the superposition diagram on the plane of (θ, x) ; **b** Three-

dimensional views of the superposition diagram on the plane of $(z, 5 \cos(0.005t), w)$

trajectories do not exit the spiking-state-oscillations-1 due to the supercritical Hopf bifurcation delay effect [42, 43]. When θ decreases to the value of θ_{LP1} , the trajectories rapidly descend to the attractive domain of limit cycle attractor $LC2$ and vibrate for the spiking-state-oscillations-2.

As θ reaches the smallest value -5 , it begins to grow. The trajectories continue oscillating in $LC2$ for the spiking-state-oscillations-2. As previously analyzed, the spiking-state-oscillations-2 are terminated on the fold bifurcation $LP2$ and the trajectories rapidly

enter the attractive domain of limit cycle attractor $LC1$ and oscillate for the spiking-state-oscillations-1.

From Fig. 4a, we may have an illusion that the two limit cycles $LC1$ and $LC2$ intersect each other, this phenomenon can be called twist of trajectories in space. Actually, these two limit cycles are independent and do not intersect in space, Fig. 4b clearly illustrates this fact. For such MMOs, the two spiking-state-oscillations are switched by twofold bifurcations, so we can name this dynamical behaviors as “fold/fold” MMOs.

4.2 “Delayed supHopf/fold-fold/fold” MMOs

Secondly, we explore the dynamical responses in area B, the related projection diagrams are shown in Fig. 5, where the parameters are chosen at $\mu = 0.5, k = 3, \alpha = 0.5, \varepsilon = 1, f = 5, \omega = 0.005$ and $\delta = 0.6$. We can find that the MMOs are related to two stable limit cycles and four spiking-state-oscillations are involved in each period. By overlapping the diagram projected onto the (θ, x) plane and the bifurcation characteristics projected onto the (θ, x) plane, we can get a clear idea on the generation of the MMOs, as displayed in Fig. 6a.

In order to analyze the generation of such MMOs in detail, we decompose a periodic motion into two parts, the first is θ slowly decreasing from $+5$ to -5 and the second is θ slowly increasing from -5 to $+5$, the corresponding diagrams are plotted in Fig. 6b, c. For the first part, the trajectories firstly move acutely for the spiking-state-oscillations-1 in the attractive domain of the limit cycle attractor $LC1$. As θ arrives at supHopf1 , the trajectories continue vibrating with a large-amplitude due to the Hopf bifurcation delay effect. After then, fold bifurcation point $LP1$ appears, resulting in the trajectories jumping into the attractive domain of $LC2$ to form the spiking-state-oscillations-2. The spiking-state-oscillations-2 will remain until θ reaches -5 due to the Hopf bifurcation delay, even if a Hopf bifurcation supHopf3 occurs at $\theta = -4.574$.

For the second part, the trajectories firstly move peacefully in the vector field of $E2$. As θ arrives at

supHopf3 , the trajectories continue moving with a small-amplitude owing to the effect of the delayed Hopf bifurcation. Sometime later, the Hopf bifurcation delay phenomenon finishes and the trajectories begin to vibrate dramatically to form the spiking-state-oscillations-3. Similarly, the spiking-state-oscillations-3 are not terminated by Hopf bifurcation supHopf2 but ended up with fold bifurcation $LC2$. The trajectories jump to oscillate in the attractive domain of $LC1$ to form the spiking-state-oscillations-4.

Figure 6d presents a fact that the two limit cycles $LC1$ and $LC2$ are independent and do not intersect in space. For such MMOs, the spiking-state-oscillations-1 and the spiking-state-oscillations-4 are induced by fold bifurcations and terminated also by fold bifurcations, while the spiking-state-oscillations-2 are produced by delayed supercritical Hopf bifurcations and ended up with fold bifurcations. So, such dynamical responses are named “delayed supHopf/fold-fold/fold” MMOs.

In area B, if we fix the parameters at $\mu = 0.5, k = 3, \alpha = 0.5, \varepsilon = 1, f = 5, \omega = 0.005$ and $\delta = 0.9$, the other MMOs’ structures are created, as displayed in Fig. 7. For such MMOs, the two spiking-state-oscillations are involved in each period. We also find that the trajectories can arrive at the vector field of $LC2$ when θ decreases through the point of the supercritical Hopf bifurcation supHopf3 and a large bifurcation delay interval can be seen as θ passes across the point of the supercritical Hopf bifurcation supHopf3 .

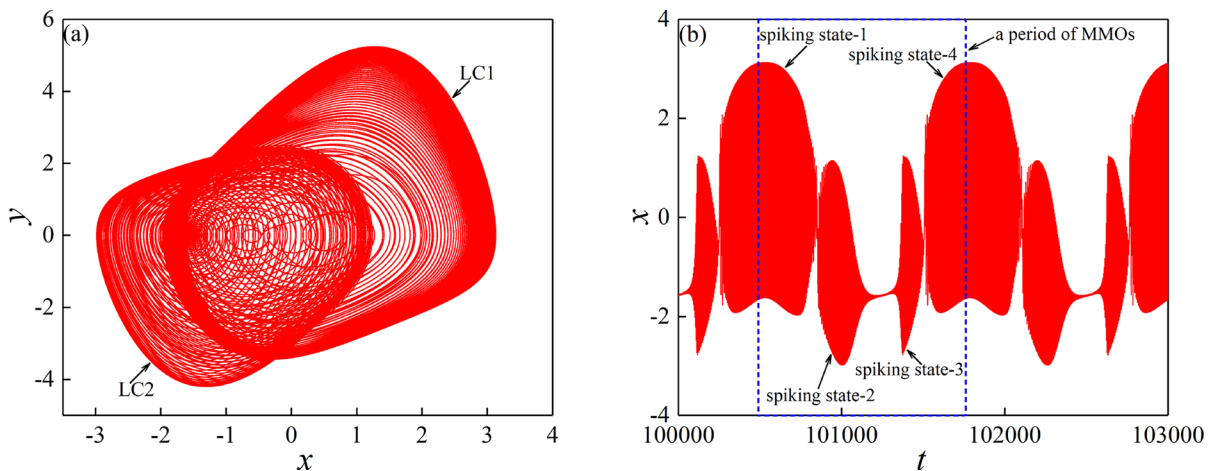


Fig. 5 The related diagrams for the fixed parameters $\mu = 0.5, k = 3, \alpha = 0.5, \varepsilon = 1, f = 5, \omega = 0.005$ and $\delta = 0.6$. **a** Diagram projected onto the (x, y) plane; **b** time histories on the plane of (t, x)

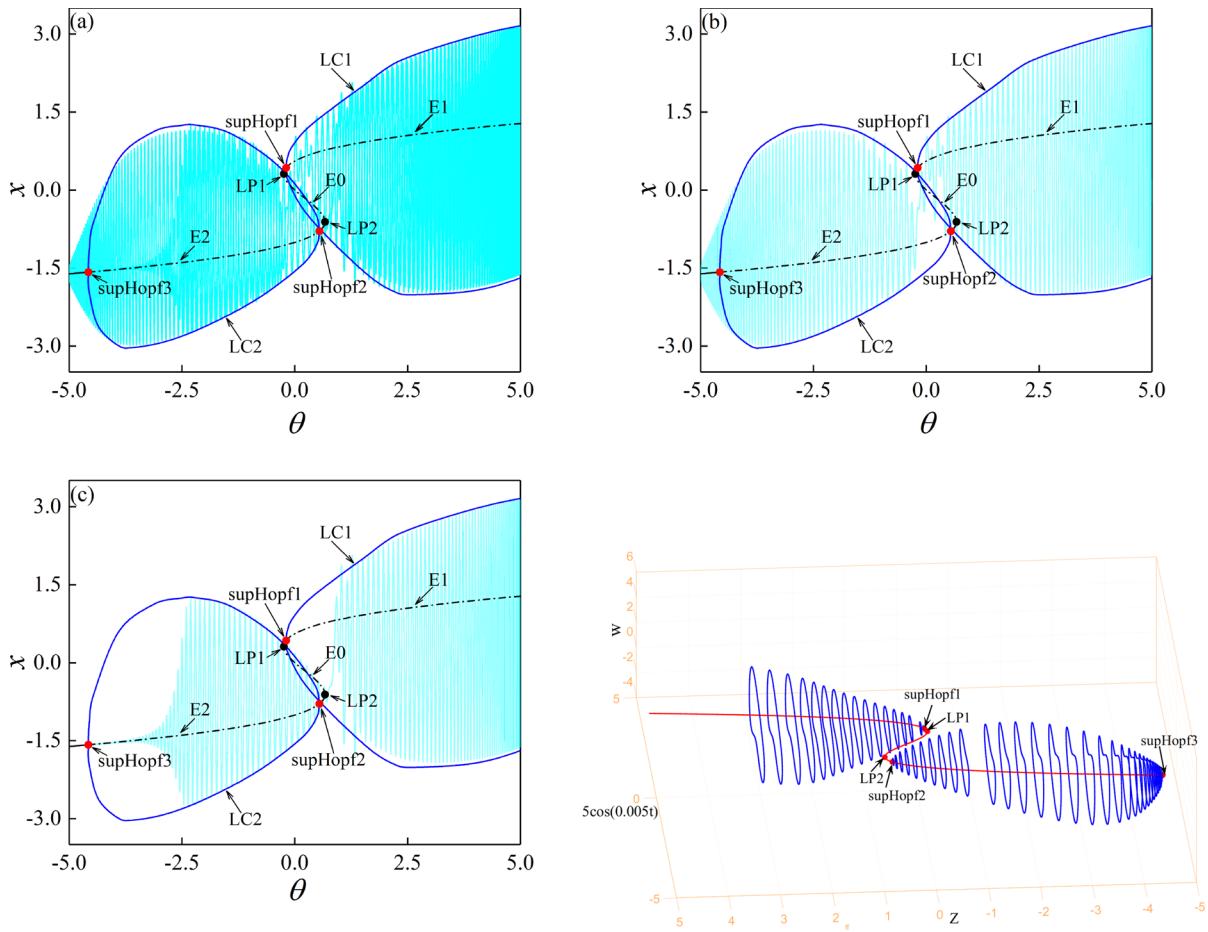


Fig. 6 Fast/slow decomposition of the MMOs for $\mu = 0.5$, $k = 3$, $\alpha = 0.5$, $\varepsilon = 1$, $f = 5$, $\omega = 0.005$ and $\delta = 0.6$. **a** Two-dimensional views of the superposition diagram projected onto the (θ, x) plane; **b** the evolution process of θ slowly varying

from $+5$ to -5 ; **c** the evolution process of θ slowly varying from -5 to $+5$; **d** three-dimensional views of the superposition diagram on the plane of $(z, 5 \cos(0.005t), w)$

According to the generation of the two spiking-state-oscillations, such dynamical responses are named “fold/fold-fold/supHopf” MMOs. In this area, we can obtain a fact that Hopf bifurcation delay plays an important action in the generation of the different MMOs.

4.3 “Fold/inverse-period-4-inverse-period-twofold limit cycle” chaotic MMOs

Thirdly, the mechanism of the dynamical responses in area C is investigated in this subsection, the corresponding diagrams are presented in Fig. 8, where the parameters are fixed at $\mu = 0.5$, $k = 3$, $\alpha = 0.5$, $\varepsilon = 1$, $f = 5$, $\omega = 0.005$ and $\delta = 1.5$. We can see that such MMOs may be induced by the trajectories moving

among the attractive domains of an equilibrium point and two stable limit cycles, and three spiking-state-oscillations are involved in each period. In addition, we also find that Fig. 8a shows the obvious chaotic characteristics. Overlapping the diagram on the plane of (θ, x) onto the bifurcation diagram, we can get a clearer idea on the mechanism of the MMOs, as displayed in Fig. 9a.

Assuming θ slowly increases from its smallest value -5 , the trajectories move in the vector field of $E2$ with small amplitude. As θ passes through the point of $subHopf3$ slowly, the subcritical Hopf bifurcation delay effect occurs, and a large delay interval can be observed. Then, θ arrives at the $LP2$ point, the quiescent-state-oscillations are terminated, and the trajectories enter the attractive domain of the limit

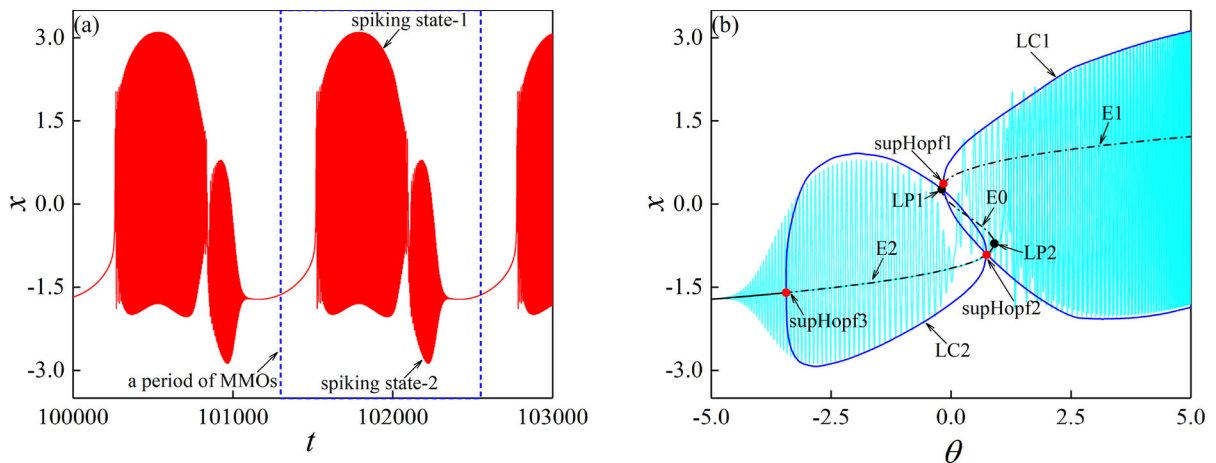


Fig. 7 Dynamical responses for $\mu = 0.5, k = 3, \alpha = 0.5, \varepsilon = 1, f = 5, \omega = 0.005$ and $\delta = 0.9$. **a** Time history on the plane of (t, x) ; **b** two-dimensional views of the superposition diagram on the plane of (θ, x)

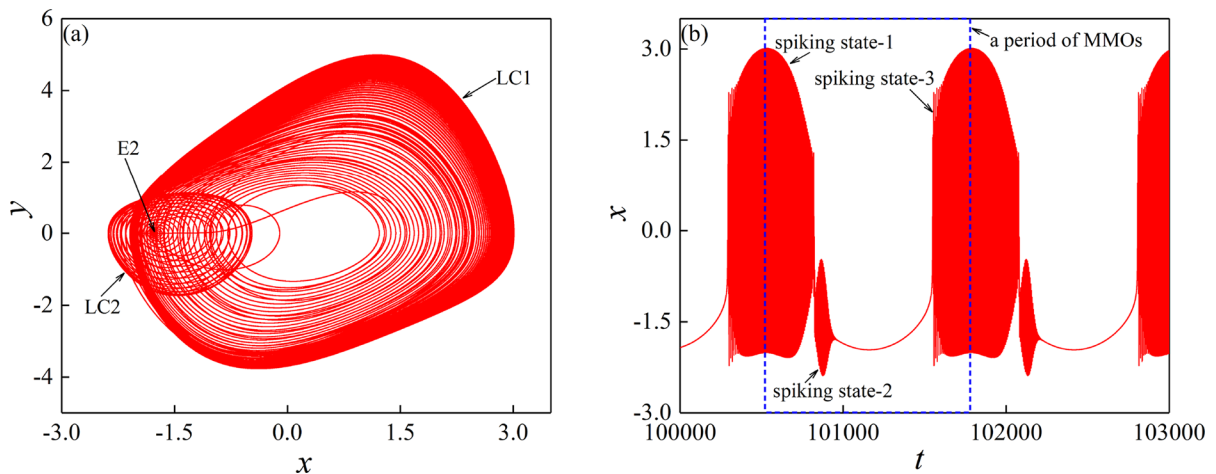


Fig. 8 The corresponding phase diagrams for the parameters $\mu = 0.5, k = 3, \alpha = 0.5, \varepsilon = 1, f = 5, \omega = 0.005$ and $\delta = 1.5$. **a** Diagram projected onto the (x, y) plane; **b** time histories on the plane of (t, x) with spiking-state-oscillations analysis

cycle attractor $LC1$, resulting in the generation of the spiking-state-oscillations-3. If θ reaches the largest value $+5$, the spiking-state-oscillations remain, and this big-amplitude vibrations can be renamed the spiking-state-oscillations-1. Sometime later, a series of period-doubling bifurcations appears, leading to the generation of chaos, and the trajectories continue vibrating with large-amplitude. Then, the system exits the chaotic behaviors by the inverse-period-doubling-bifurcation-4, and the trajectories vibrate for the period-doubling-4-oscillations. In addition, we note that the upper vibration boundary of the trajectories gradually decreases for the period-doubling-4-oscillations. While if θ arrives at the inverse-period-

doubling-bifurcation-2 point, the trajectories jump to oscillate in the vector field of the limit cycle attractor $LC2$ conveniently, resulting in the occurrence of the spiking-state-oscillations-2. As θ slowly comes across the LPC point, limit cycle $LC1$ is canceled, but due to the bifurcation delay phenomenon, the trajectories continue vibrating with big-amplitude for sometime. Subsequently, the oscillating amplitude of the trajectories decreases gradually, and the trajectories settle down to the vector field of $E2$. If θ returns to the smallest value -5 , it starts to increase, and the next chaotic MMOs begin.

For such MMOs, the spiking-state-oscillations-1–3 are induced by fold bifurcation and ended up with

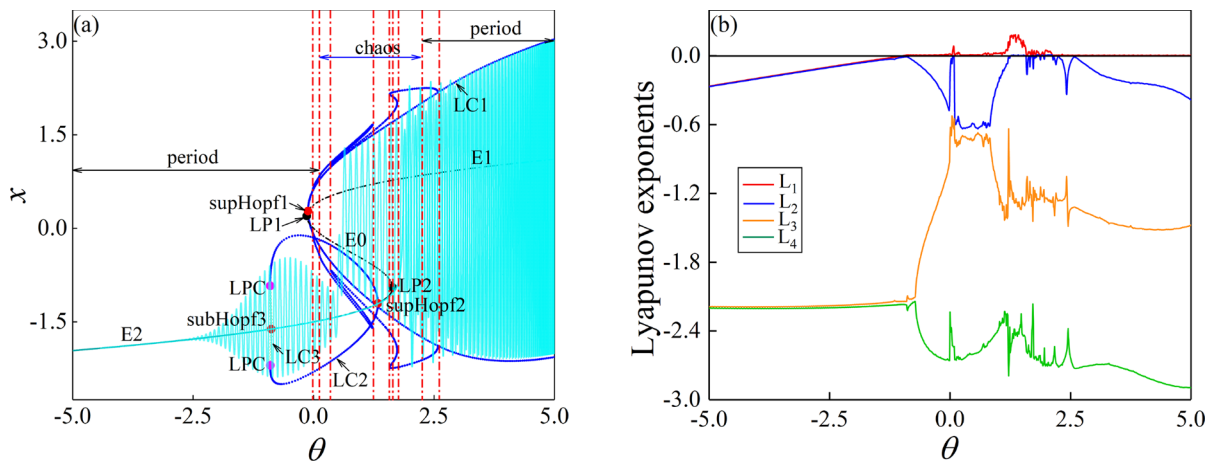


Fig. 9 Generation analysis of the MMOs for $\mu = 0.5, k = 3, \alpha = 0.5, \varepsilon = 1, f = 5, \omega = 0.005$ and $\delta = 1.5$. **a** The overlay diagram between the diagram on the plane of (θ, x) and the bifurcation diagram; **b** the Lyapunov exponent diagram

inverse-period-doubling-bifurcation-4, and the spiking-state-oscillations-2 is created by inverse-period-doubling-bifurcation-2 and terminated by fold bifurcations of limit cycles. Therefore, such MMOs can be known as “fold/inverse-period-4-inverse-period-two-fold limit cycle” MMOs.

4.4 “Fold/inverse-period-8/supHopf” chaotic MMOs

Fourthly, the parameters $\mu = 0.5, k = 3, \alpha = 0.5, \varepsilon = 1, f = 5, \omega = 0.005$ and $\delta = 1.75$ are fixed as example to explore the nonlinear responses in area D, the related diagrams are displayed in Fig. 10. We note

that the diagrams shown in Fig. 10 are similar to that in Fig. 8, but in fact, from the bifurcation structures plotted in Fig. 2d, e, we know there are qualitative differences of the generation mechanisms between them. Now, we overlap the diagram on the plane of (θ, x) onto the bifurcation diagram to present the mechanism for such MMOs, as displayed in Fig. 11.

Supposing θ slowly adds from the largest value -5 , the trajectories trace in the vector field of E_2 with small-amplitude. As θ varies through the $supHopf3$ point, the small-amplitude oscillations continue due to the Hopf bifurcation delay, and they are terminated by the $LP2$ point. Subsequently, the trajectories enter the vector field of the chaotic attractor that is created by

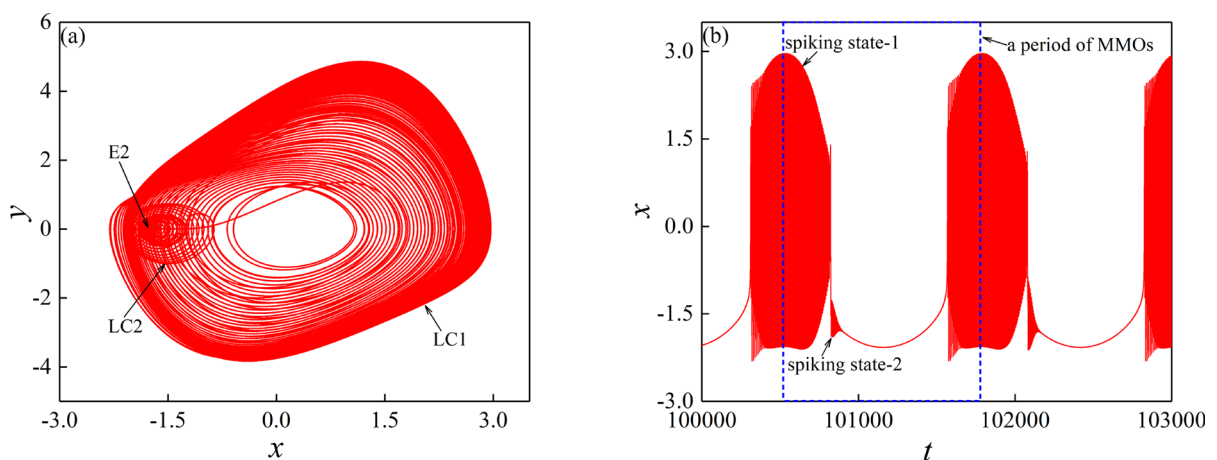


Fig. 10 The related diagrams for the parameters $\mu = 0.5, k = 3, \alpha = 0.5, \varepsilon = 1, f = 5, \omega = 0.005$ and $\delta = 1.75$. **a** Diagram projected onto the (x, y) plane; **b** Time histories on the plane of (t, x)

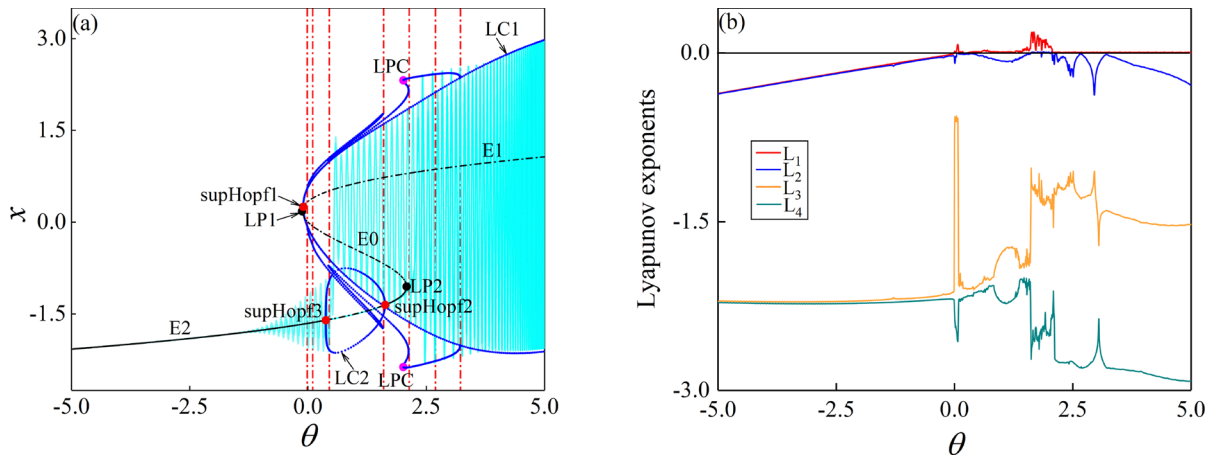


Fig. 11 Fast/slow decomposition of the MMOs for $\mu = 0.5, k = 3, \alpha = 0.5, \varepsilon = 1, f = 5, \omega = 0.005$ and $\delta = 1.75$. **a** The overlay diagram between the diagram on the plane of (θ, x) and the bifurcation diagram; **b** the Lyapunov exponent diagram

the period-doubling route. Then, the spiking-state-oscillations-1 is induced, and it will last for a long time. As θ decreases through the inverse-period-doubling-bifurcation-8 point, the chaotic behaviors are terminated, and the trajectories approach the attractive domain of the $LC2$ attractor on the lower branch. The spiking-state-oscillations-2 is created, in fact, the spiking-state-oscillations-2 can be treated as a continuation of the spiking-state-oscillations-1, just a jumping behavior induced by the inverse-period-doubling-bifurcation-8 point occurs between them. When θ decreases through the $\text{supHopf}3$ point, the trajectories' oscillating-amplitude decreases gradually, and the trajectories stabilize in the attractive domain of $E2$ to vibrate.

For such MMOs, the spiking-state-oscillations-1 and the spiking-state-oscillations-2 can be treated as a whole spiking-state-oscillation, and the whole spiking-state-oscillation involves three dynamical behaviors, i.e., fold bifurcation, inverse-period-doubling-bifurcation-8 and supercritical Hopf bifurcation. Moreover, the chaos are observed in such MMOs, so such dynamical responses are known as “fold/inverse-period-doubling-8/supHopf” MMOs.

4.5 “Fold/delayed fold limit cycle” chaotic MMOs

In this subsection, we will present a kind of chaotic MMOs in area E by taking the parameters $\mu = 0.5, k = 3, \alpha = 0.5, \varepsilon = 1, f = 5, \omega = 0.005$ and $\delta = 2$ as

a representative, and the diagram projected onto the (x, y) plane and time histories are presented in Fig. 12a, b. We can see that such MMOs behave in obvious chaotic characteristics from Fig. 12b, c. By overlying the diagram projected on the (θ, x) plane and the bifurcation diagram displayed on the (θ, x) space, we can obtain a clearer idea on such MMOs, as presented in Fig. 12d.

Supposing θ slowly adds from the smallest value -5 , the trajectories trace peacefully for a small-amplitude vibration in the vector field of $E2$, behaving in the quiescent-state-oscillations. Then, the $LP2$ point appears, resulting in the generation of a jump phenomenon. The trajectories start to vibrate violently, resulting in the appearance of the spiking-state-oscillations, and they will last for a long time. Noting that the chaotic behaviors are involved in the bifurcation structures and the trajectories have the ability to traverse the chaotic area. Subsequently, the trajectories exit the chaotic oscillations by period-doubling bifurcations and enter the period area, resulting in the period-doubling oscillations. As θ arrives the fold bifurcations of limit cycles, the stability of $LC1$ is changed. On the upper curve, no attractive domain of any stable attractors exists, the trajectories can only choose to vibrate in the unstable vector field of $LC1$ due to the bifurcation delay effect. Sometime later, the trajectories jump to vibrate in the vector field of $E2$ and the quiescent-state-oscillations are produced on the lower curve.

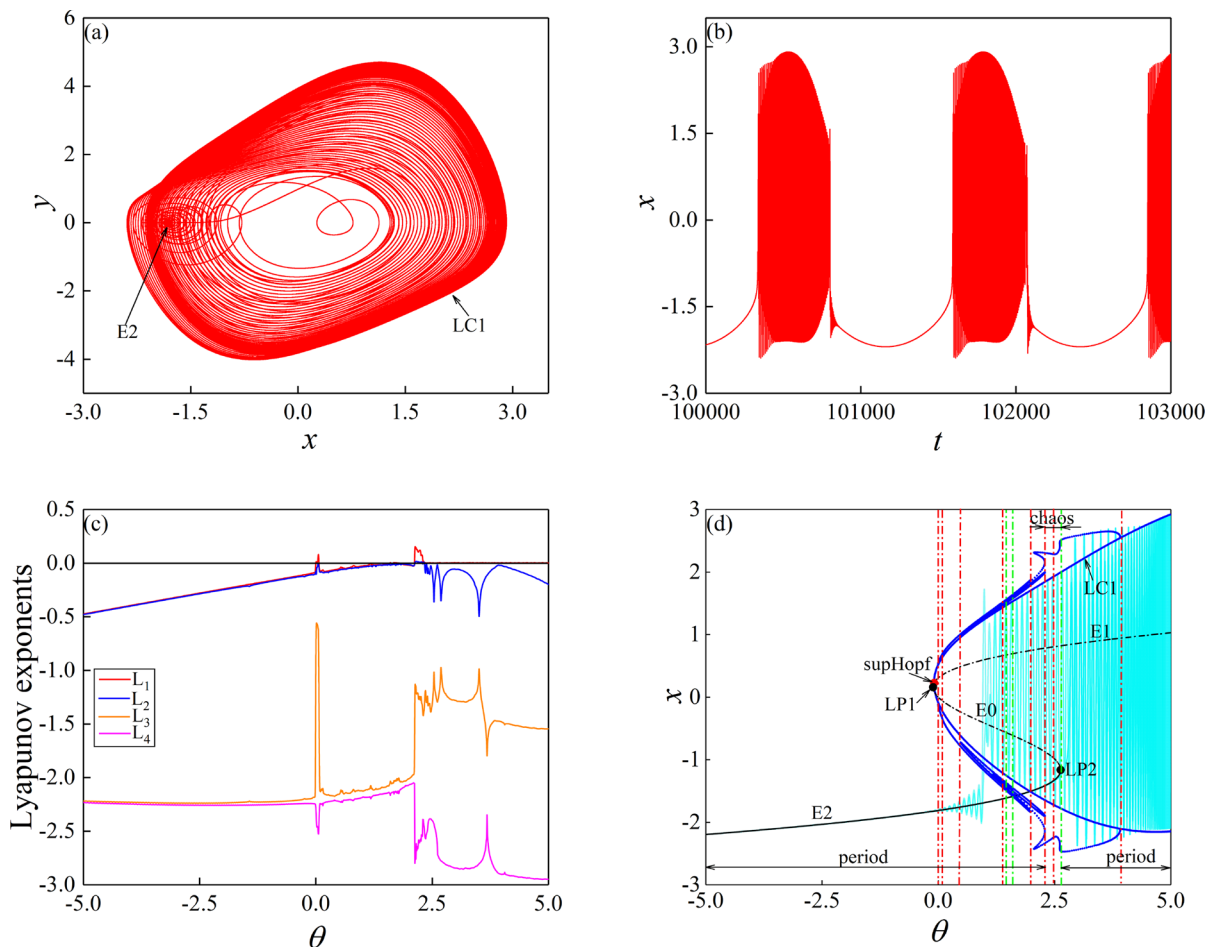


Fig. 12 Phase diagrams and fast/slow decomposition of the MMOs for the values of $\mu = 0.5$, $k = 3$, $\alpha = 0.5$, $\varepsilon = 1$, $f = 5$, $\omega = 0.005$ and $\delta = 2$. **a** Diagram projected onto the (x, y) plane; **b** time histories on the plane of (t, x) ; **c** maximum Lyapunov

exponent diagram; **d** Fast/slow analysis by superposing the diagram projected onto the (θ, x) plane to the bifurcation diagram on the (θ, x) space

For such MMOs, the spiking-state-oscillations are produced by fold bifurcations and terminated by the delayed fold bifurcations of limit cycles, and chaos can be observed. Therefore, the dynamical responses are named “fold/delayed fold limit cycle” chaotic MMOs.

4.6 “Fold/fold limit cycle” periodic MMOs

In the last subsection, we will analyze a period MMOs’ type in area E, the related diagrams are shown in Fig. 13, where the parameters are taken at $\mu = 0.5$, $k = 3$, $\alpha = 0.5$, $\varepsilon = 1$, $f = 5$, $\omega = 0.005$ and $\delta = 2.6$. We can see that the MMOs are created by the trajectories switching between the equilibrium point

and limit cycle, and only one spiking-state-oscillations-1 is involved in each period. The mechanism of such MMOs can be explored clearly by superposing the diagram projection onto the (θ, x) plane onto the bifurcation diagram displayed on the (θ, x) space, as displayed in Fig. 14a.

We also assume θ slowly increases from the smallest value -5 , the trajectories trace gently for a small-amplitude vibration in the vector field of $E2$, agreeing with the quiescent-state-oscillations. As θ arrives at the $LP2$ point, a jump phenomenon occurs, resulting in the trajectories getting into the attractive domain of $LC1$, and the spiking-state-oscillations-1 can be observed. Sometime later, θ reaches the maxima value $+5$, it begins to decrease, but the

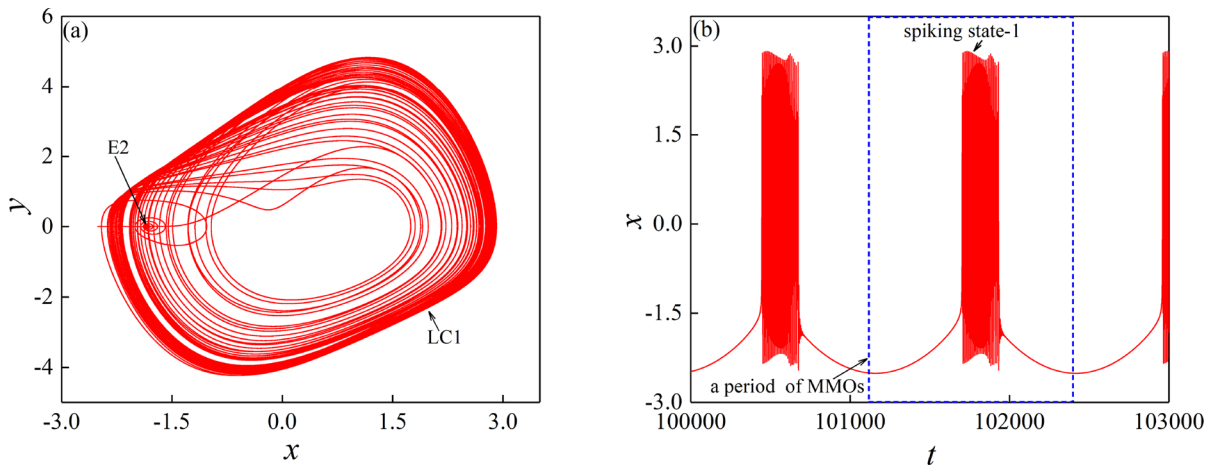


Fig. 13 The corresponding diagrams for the parameters are $\mu = 0.5$, $k = 3$, $\alpha = 0.5$, $\varepsilon = 1$, $f = 5$, $\omega = 0.005$ and $\delta = 2.6$. **a** Diagram projection onto the (x, y) plane; **b** time histories on the plane of (t, x)

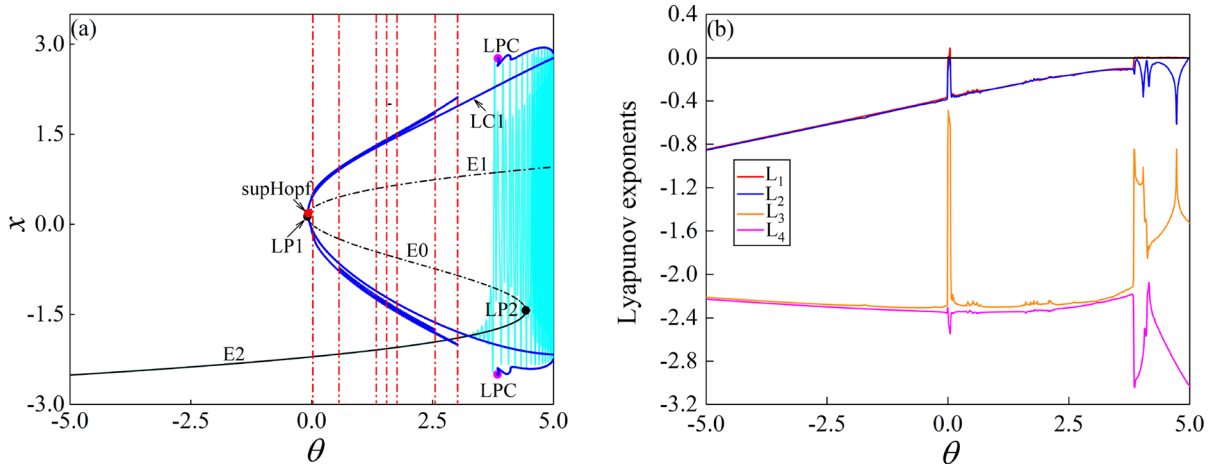


Fig. 14 Fast/slow decomposition of the MMOs for $\mu = 0.5$, $k = 3$, $\alpha = 0.5$, $\varepsilon = 1$, $f = 5$, $\omega = 0.005$ and $\delta = 2.6$. **a** The overlay diagram between the bifurcation diagram and the

diagram projected onto the plane of (θ, x) ; **b** the maximum Lyapunov exponent diagram

spiking-state-oscillations-1 still continues. While if θ decreases to the *LPC* point, no stable limit cycle attractor exists, the trajectories have no choice but to jump to the attractive domain of the equilibrium point *E2* on the lower curve, resulting in the generation of the quiescent-state-oscillations.

For such MMOs, the spiking-state-oscillations-1 is produced by fold bifurcations and terminated at fold bifurcations of limit cycles, and periodic characteristics can be observed from Fig. 14b. Therefore, the dynamical responses shown in Fig. 13 are called “fold/fold limit cycle” periodic MMOs.

5 Conclusions and discussions

The study of MMOs in high-dimensional systems is one of the hot spots in the fast/slow dynamics. In this paper, we take a coupled Duffing–Van der Pol model with a slowly changing periodic external forcing as an example to investigate the generation of the complex MMOs, where the bifurcation delay phenomenon and twist of trajectories in space can be observed. As soon as the trajectories undergo a jump phenomenon to the periodic limit cycles or chaotic limit cycles, periodic or chaotic MMOs can be observed. Furthermore, the mechanisms of the periodic and chaotic MMOs are

investigated by using the phase diagrams, time series, maximum Lyapunov exponent diagrams, three-dimensional phase diagrams and superimposed diagrams.

Our study shows that the bifurcation delay phenomenon can lead to the trajectories to arrive at the attractive domain of different attractors, which can be used to explore the generation of the different spiking-state-oscillations. Moreover, we find that the chaotic attractor is induced by the period-doubling route, and the trajectories have their own choice to cross or not cross the chaotic area. Our results provide more possible routes to the MMOs and improve a better understanding of the bifurcation structures and bifurcation delay on the generation of the MMOs.

Acknowledgements This paper is supported by the National Natural Science Foundation of China (Grant No. 12002299) and Natural Science Foundation for colleges and universities in Jiangsu Province (Grant No. 20KJB110010).

Funding Funding for this study was obtained from the National Natural Science Foundation of China (Grant No. 12002299) and the Natural Science Foundation for Colleges and Universities in Jiangsu Province (Grant No. 20KJB110010).

Data availability The datasets generated during and/or analyzed during the current study are available from the corresponding author on reasonable request.

Declarations

Conflict of interest The authors declare that there is no conflict of interest.

References

1. Taher, H., Avitabile, D., Desroches, M.: Bursting in a next generation neural mass model with synaptic dynamics: a slow-fast approach. *Nonlinear Dyn.* **108**(4), 4261–4285 (2022)
2. Bashkirtseva, I., Ryashko, L.: Transformations of spike and burst oscillations in the stochastic Rulkov model. *Chaos Solitons Fractals* **170**, 113414 (2023)
3. Bonet, C., Jeffrey, M.R., Martin, P., Olm, J.M.: Novel slow-fast behaviour in an oscillator driven by a frequency-switching force. *Commun. Nonlinear Sci. Numer. Simul.* **118**, 107032 (2023)
4. Sekikawa, M., Kousaka, T., Tsubone, T., Inaba, N., Okazaki, H.: Bifurcation analysis of mixed-mode oscillations and Farey trees in an extended Bonhoeffer–Van der Pol oscillator. *Physica D* **433**, 133178 (2022)
5. Cohen, N., Bucher, I., Feldman, M.: Slow-fast response decomposition of a bi-stable energy harvester. *Mech. Syst. Signal Process.* **31**, 29–39 (2012)
6. Ma, X.D., Zhang, X.F., Yu, Y., Bi, Q.S.: Compound bursting behaviors in the parametrically amplified Mathieu–Duffing nonlinear system. *J. Vib. Eng. Technol.* **10**, 95–110 (2022)
7. Doedel, E.J., Pando, C.L.: Correlation sum scalings from mixed-mode oscillations in weakly coupled molecular lasers. *Chaos* **32**(8), 083132 (2022)
8. Doedel, E.J., Pando, C.L.: Multiparameter bifurcations and mixed-mode oscillations in Q-switched CO₂ lasers. *Phys. Rev. E* **89**(5), 052904 (2014)
9. Desroches, M., Guillamon, A., Ponce, E., Prohens, R., Rodrigues, S., Teruel, A.E.: Canards, folded nodes, and mixed-mode oscillations in piecewise-linear slow-fast systems. *SIAM Rev.* **58**(4), 653–691 (2016)
10. Lin, Y., Liu, W.B., Hang, C.: Revelation and experimental verification of quasi-periodic bursting, periodic bursting, periodic oscillations in third-order non-autonomous memristive FitzHugh–Nagumo neuron circuit. *Chaos Solitons Fractals* **167**, 113006 (2023)
11. Zhao, F., Ma, X.D., Cao, S.Q.: Periodic bursting oscillations in a hybrid Rayleigh–Van der Pol–Duffing oscillator. *Nonlinear Dyn.* **111**(3), 2263–2279 (2023)
12. Huang, J.J., Bi, Q.S.: Bursting oscillations with multiple modes in a vector field with triple Hopf bifurcation at origin. *J. Sound Vib.* **545**, 117422 (2023)
13. Hua, H.T., Gu, H.G., Jia, Y.B., Lu, B.: The nonlinear mechanisms underlying the various stochastic dynamics evoked from different bursting patterns in a neuronal model. *Commun. Nonlinear Sci. Numer. Simul.* **110**, 106370 (2022)
14. Saha, T., Pal, P.J., Banerjee, M.: Slow-fast analysis of a modified Leslie–Gower model with Holling type I functional response. *Nonlinear Dyn.* **108**(4), 4531–4555 (2022)
15. Van der Pol, B.: On relaxation-oscillations. *Lond. Edinb. Dublin Philos. Mag. J. Sci. Ser.* **2**(11): 978–992 (1926)
16. Simo, H., Tchendjeu, A.E.T., Kenmogne, F.: Study of bursting oscillations in a simple system with signum nonlinearity with two timescales: theoretical analysis and FPGA implementation. *Circuits Syst. Signal Process.* **41**(8), 4185–4209 (2022)
17. Chen, M., Qi, J.W., Wu, H.G., Xu, Q., Bao, B.C.: Bifurcation analyses and hardware experiments for busting dynamics in non-autonomous memristive FitzHugh–Nagumo circuit. *Sci. China Technol. Sci.* **63**(6), 1035–1044 (2020)
18. Ma, X.D., Bi, Q.S., Wang, L.F.: Complex periodic bursting structures in the Rayleigh–Van der Pol–Duffing oscillator. *J. Nonlinear Sci.* **32**(2), 25 (2022)
19. Baldemir, H., Avitabile, D., Tsaneva-Atanasova, K.: Pseudo-plateau bursting and mixed-mode oscillations in a model of developing inner hair cells. *Commun. Nonlinear Sci. Numer. Simul.* **80**, 104979 (2020)
20. Krupa, M., Vidal, A., Desroches, M., Clément, F.: Mixed-mode oscillations in a multiple time scale phantom bursting system. *SIAM J. Appl. Dyn. Syst.* **11**(4), 1458–1498 (2012)
21. Battaglin, S., Pedersen, M.G.: Geometric analysis of mixed-mode oscillations in a model of electrical activity in human beta-cells. *Nonlinear Dyn.* **104**(4), 4445–4457 (2021)

22. Desroches, M., Kaper, T.J., Krupa, M.: Mixed-mode bursting oscillations: dynamics created by a slow passage through spiking-adding canard explosion in a square-wave burster. *Chaos* **23**(4), 046106 (2013)
23. Inaba, N., Kousaka, T.: Nested mixed-mode oscillations. *Physica D* **401**, 132152 (2020)
24. Sharma, J., Tiwari, I., Parmananda, P., Rivera, M.: Aperiodic bursting dynamics of active rotors. *Phys. Rev. E* **105**(1), 014216 (2022)
25. Liu, Y.R., Liu, S.Q.: Characterizing mixed-mode oscillations shaped by canard and bifurcation structure in a three-dimensional cardiac cell model. *Nonlinear Dyn.* **103**(3), 2881–2902 (2021)
26. Kouayep, R.M., Talla, A.F., Mbé, J.H.T., Woafu, P.: Bursting oscillations in Colpitts oscillator and application in optoelectronics for the generation of complex optical signals. *Opt. Quant. Electron.* **52**(6), 291 (2020)
27. Bao, B.C., Yang, Q.F., Zhu, L., Bao, H., Xu, Q., Chen, M.: Chaotic bursting dynamics and coexisting multistable firing patterns in 3D autonomous Morris-Lecar model and microcontroller-based validations. *Int. J. Bifurc. Chaos* **29**(10), 1950134 (2019)
28. Zhang, Y.T., Cao, Q.J., Huang, W.H.: Bursting oscillations of the perturbed quasi-zero stiffness system with positive/negative stiffness at origin. *Physica D* **445**, 133643 (2023)
29. Zhang, C., Tang, Q.X., Wang, Z.X.: Pulse-shaped explosion-induced and non-pulse-shaped explosion-induced bursting dynamics in a parametrically and externally forced Rayleigh-Van der Pol oscillator. *Nonlinear Dyn.* **111**(7), 6199–6211 (2023)
30. Han, X.J., Bi, Q.S.: Bursting oscillations in Duffing's equation with slowly changing external forcing. *Commun. Nonlinear Sci. Numer. Simul.* **16**(10), 4146–4152 (2011)
31. Huang, J.J., Bi, Q.S.: Mixed-mode bursting oscillations in the neighborhood of a triple Hopf bifurcation point induced by parametric low-frequency excitation. *Chaos Solitons Fractals* **166**, 113016 (2023)
32. Kpomahou, Y.J.F., Adéchinan, J.A., Ngounou, A.M., Yamadjako, A.E.: Bursting, mixed-mode oscillations and homoclinic bifurcation in a parametrically and self-excited mixed Rayleigh–Lienard oscillator with asymmetric double well potential. *Pramana* **96**(4), 176 (2022)
33. Vijay, S.D., Ahamed, A.I., Thamilmaran, K.: Distinct bursting oscillations in parametrically excited Lienard system. *AEU-Int. Electron. Commun.* **156**, 154397 (2022)
34. Oyeleke, K.S., Olusola, O.I., Kolebaje, O.T., Vincent, U.E., Adeloye, A.B., McClintock, P.V.E.: Novel bursting oscillations in a nonlinear gyroscope oscillator. *Phys. Scr.* **97**(8), 085211 (2022)
35. Balamurali, R., Kengne, J., Chengui, R.G., Rajagopal, K.: Coupled Van der Pol and Duffing oscillators: emergence of antimonotonicity and coexisting multiple self-excited and hidden oscillations. *Eur. Phys. J. Plus* **137**(7), 789 (2022)
36. Woafu, P., Chedjou, J.C., Fotsin, H.B.: Dynamics of a system consisting of a Van der Pol oscillator coupled to a duffing oscillator. *Phys. Rev. E* **54**(6), 5929–5934 (1996)
37. Kadji, H.E., Yamapi, R.: General synchronization dynamics of coupled Van der Pol–Duffing oscillators. *Physica A* **370**(2), 316–328 (2006)
38. Kuznetsov, A.P., Stankevich, N.V., Turukina, L.V.: Coupled Van der Pol–Duffing oscillator: phase dynamics and structure of synchronization tongues. *Physica D* **238**(14), 1203–1215 (2009)
39. Liu, X., Zhang, T.H.: Bogdanov–Takens and triple zero bifurcations of coupled Van der Pol–Duffing oscillators with multiple delays. *Int. J. Bifurc. Chaos* **27**(9), 1750133 (2017)
40. Bourafa, S., Abdelouahab, M.S., Moussaoui, A.: On some extended Rough-Hurwitz conditions for fractional-order autonomous systems of order α is an element of $(0,2)$ and their applications to some population dynamic models. *Chaos Solitons Fractals* **133**, 109623 (2020)
41. Kuznetsov, Y.A.: *Elements of Applied Bifurcation Theory*. Springer, New York (1995)
42. Zhao, H.Q., Ma, X.D., Yang, W.J., Zhang, Z., Bi, Q.S.: The mechanism of periodic and chaotic bursting patterns in an externally excited memcapacitive system. *Chaos Solitons Fractals* **171**, 113407 (2023)
43. Zhou, C.Y., Li, Z.J., Xie, F., Ma, M.L., Zhang, Y.: Bursting oscillations in Sprott B system with multi-frequency slow excitations: two novel “Hopf/Hopf”-hysteresis-induced bursting and complex AMB rhythms. *Nonlinear Dyn.* **97**(4), 2799–2811 (2019)

Publisher's Note Springer Nature remains neutral with regard to jurisdictional claims in published maps and institutional affiliations.

Springer Nature or its licensor (e.g. a society or other partner) holds exclusive rights to this article under a publishing agreement with the author(s) or other rightsholder(s); author self-archiving of the accepted manuscript version of this article is solely governed by the terms of such publishing agreement and applicable law.